



URANS Simulation of Self-Recirculation Casing Treatment in a Transonic Compressor

M. J. Shahriyari and H. Khaleghi[†]

Department of Aerospace Engineering, Amirkabir University of Technology, Tehran, 15875-4413, Iran

[†]Corresponding Author Email: khaleghi@aut.ac.ir

ABSTRACT

Time-accurate numerical calculations are performed to investigate the effect of air recirculation on NASA Rotor 37. An annular casing-mounted recirculation passageway is designed and located over the blades. Because the investigated rotor does not have any stator, the bleed air has a high circumferential velocity component (in the same direction of the rotor). Therefore, the injected air would have a high swirl component, reducing the injection's effectiveness. As a result, anti-swirl blades have been installed within the recirculation duct, to reduce flow swirl and improve injector effectiveness. Different anti-swirl vanes have been simulated in order to determine the best vanes in terms of minimum pressure loss and zero injection yaw angle (axial injection). Results show that these vanes can effectively turn the circulated fluid to the axial direction and provide a high velocity axial injection upstream of the rotor blades. As a result of the effective injection, the leakage flow moves downstream, improving stability by shifting the stalling point to lower mass flow rates. Because the injection port is close to the blade, the interaction of the passage shock and the injection port causes unsteadiness in the injection mass flow, which is discussed in the paper.

Article History

Received July 22, 2023

Revised November 8, 2023

Accepted December 4, 2023

Available online February 24, 2024

Keywords:

Recirculation

NASA Rotor-37

Injection

Bleed

Anti-swirl vanes

1. INTRODUCTION

There is a continuous effort to improve the performance of aero compressors (Yang et al., 2019; Xiang et al., 2021; Tang et al., 2022). The leakage flow from the tip of the blades is known to reduce the compressor performance and its operability (Puterbaugh & Brendel, 1997; Jahani et al., 2022). This gives a strong motivation to employ passive and active methods to control the tip clearance flow. One of these methods involves fluid injection upstream of a compressor blade, which reduces endwall blockage, and consequently, enhances the compressor operating range. Many researchers have studied the effect of tip injection on compressor stability. Weigl et al. (1997) showed that most of improvement in the compressor stability is related to steady injection. Suder et al. (2001) investigated the effect of injection velocity on the performance of an axial compressor rotor. They used discrete injectors and showed that the stability enhancement increases by increasing the injection speed and the circumferential extension of the injectors. Wang et al. (2018) investigated (experimentally and numerically) the effects of tip injection on the performance of a subsonic compressor. An optimum

injection frequency was found by Zhou et al. (2010) which maximized the compressor range extension. The effects of injection angle (Khaleghi et al. 2008) and the size of the injector in the radial direction (Khaleghi, 2017), have also been studied. Results showed that maximum stability was achieved at zero radial angle and a circumferential angle opposite to the blade rotation.

In recirculation casing treatment approach, air is circulated over a compressor stage (or rotor) through a pipe or passageway. This method can improve the compressor operability, with less efficiency loss than other casing treatment concepts (Hathway, 2002). Freeman et al. (1998) studied steady and controlled recirculation on stall control of a turbojet engine. The controlled recirculation was found to be more effective. The impacts of steady/unsteady recirculation were investigated on the stability a multi stage compressor by Strazisar et al. (2004), which indicated that unsteady recirculation was more beneficial. Recessed vane casing treatment was studied by Azimian et al. (1990) and Akhlaghi et al. (2003). The stability was increased without efficiency loss. Khaleghi et al. (2007) conducted steady calculations to investigate the impact of annular recirculation on a transonic compressor rotor (NASA Rotor-67). The

recirculation channel was equipped with anti-swirl blades. Considerable enhancement in the compressor stability was achieved (at the expense of some efficiency loss). Khaleghi (2014) investigated discrete recirculation on a transonic fan. Wang et al. (2018) studied recirculation casing treatment on a subsonic compressor, which showed stability improvement. A numerical study of the application of a so called “feedback channel” on NASA Stage 37 was reported by Dinh et al. (2017). The rotor stability was considerably increased, but at the expense of efficiency penalty.

Several new designs have been proposed and investigated in recent years for self-recirculating methods, for example (Khaleghi, 2020; Yan & Chu, 2020; Vuong & Kim, 2021). Vuong and Kim (2021) studied the effects of a dual bleeding port recirculation channel on the performance of NASA Stage 37 transonic compressor and optimized the channel’s configuration, in order to improve the compressor’s operating range. The optimum design was shown to enhance the stall margin by 51.36 percent, at the expense of some performance loss, when compared to no recirculation case. Yan and Chu (2020) used numerical simulation to investigate a new method of self-recirculating casing treatment with double-bleed ports on NASA Rotor-37. Results showed that the use of double-bleed port self-recirculating approach reduces blade tip load and weakens the blade tip blockage, hence improves stall margin of the rotor. Khaleghi (2020) presented a new self-recirculating approach and numerically evaluated it on NASA Rotor-67. In his approach, air is taken from downstream of the rotor and is injected over portion of the blade in the circumferential direction (in opposite direction of the blade rotation). It is demonstrated that the endwall recirculation used does not reduce the incidence angle upstream of the blade, but reduces the pressure difference between the pressure and suction surface, pushing the leakage vortex and the passage shock downstream and increasing the rotor operating range.

Although annular recirculation casing treatment has been investigated by some researchers, it still needs more numerical and experimental investigations before being used in a real application. The main goal of this study is to extend the knowledge on recirculation casing treatment. Furthermore, URANS simulations are performed in the current study (using the three dimensional CFD code, CFX), because a number of researchers emphasized the importance of endwall flow unsteadiness at the presence of casing treatment and endwall injection (e.g., Lim et al. (2011); Hwang and Kang (2013); Khaleghi (2014) and Khaleghi et al. (2021)).

2. CONFIGURATION AND NUMERICAL DETAILS

All of the simulations have been conducted on NASA Rotor 37, which was originally designed and tested at NASA Lewis Research Center (Reid & Moore, 1978, 1979). The design characteristic values of this transonic axial compressor rotor are given in Table 1. The focus of the current work is the stable operation of the compressor up to near-stall point, and therefore, the computational domains in both the smooth and recirculation casings contain only one of the blades (except the optimum

Table 1 NASA Rotor-37 design characteristic values

Characteristic	Value
Number of blades	36
Tip Solidity	1.288
Inlet hub/tip diameter ratio	0.7
Aspect ratio	1.19
Tip relative inlet Mach number	1.48
Hub relative inlet Mach number	1.13
Design tip clearance (mm)	0.356
Choking mass flow rate (Kg/s)	20.93
Tip Speed (m/s)	454.13

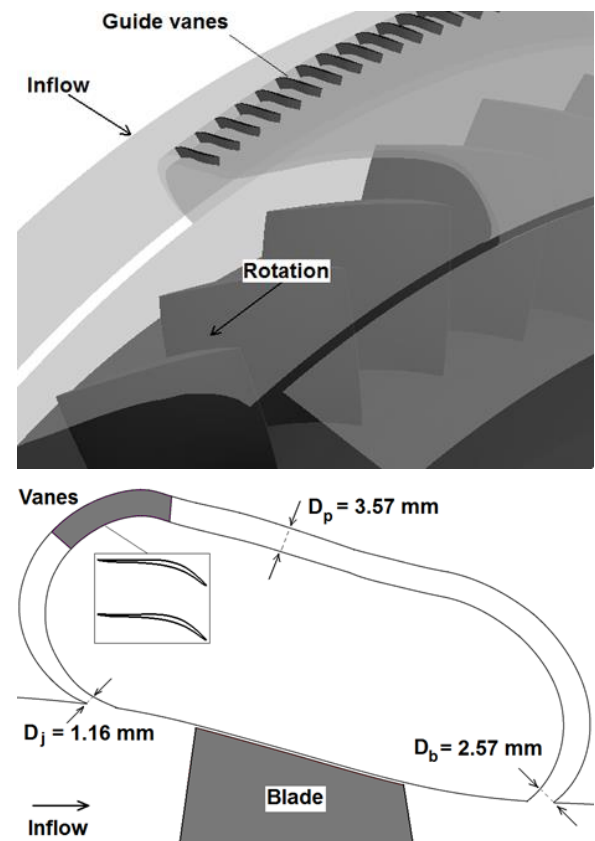


Fig. 1 Geometry and configuration of the annular recirculation passageway

recirculation, which is simulated by using three passages). Figure 1 shows the geometrical details and the configuration of the annular recirculation passageway with respect to the blades. The bleed port is located at about 66 percent tip axial chord downstream of the blade trailing-edge. The location of the injection port with respect to the blade leading-edge is about 45 percent tip axial chord upstream. These locations are chosen by considering the previous studies on recirculation casing treatment (e.g., Khaleghi et al. (2007)). The bleed throat (D_b) is designed to be about 2.2 times, and the passage height (D_p) three times larger than the injection throat (D_j), with the expectation to reduce the passageway diffusion loss. Because there is no stator or outlet vanes, the bled air has a high circumferential velocity component in the same direction of the rotor rotation. This reduces the injector

Table 2 Configurations

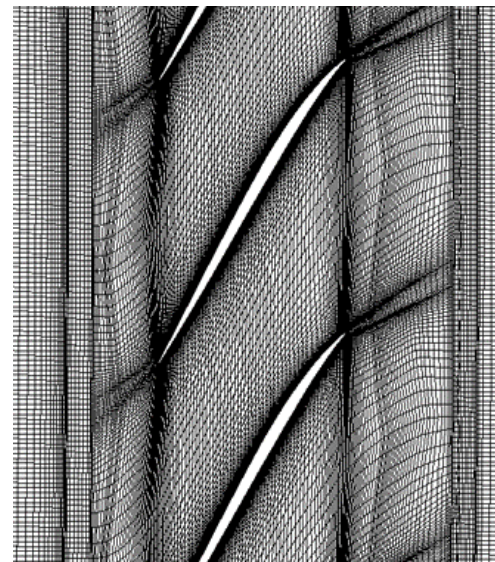
Number of vanes	Solidity
36	0.333
72	0.667
144	1.333
216	2.0
288	2.667
360	3.333

effectiveness, because the air would be injected at the injection face with a low relative velocity. Therefore, anti-swirl vanes were designed and inserted into the recirculation passageway. The geometry of the vanes is similar to that applied by Talebnezhad (2017). Numerical computations have been performed for six solidities of the anti-swirl vanes (Table 2), in order to find the optimum number of guide vanes in terms of maximum effectiveness and minimum pressure loss. For the optimum recirculation case, three-passageway simulations have been performed, in order to accurately predict the near-stall condition, which is not periodic in nature.

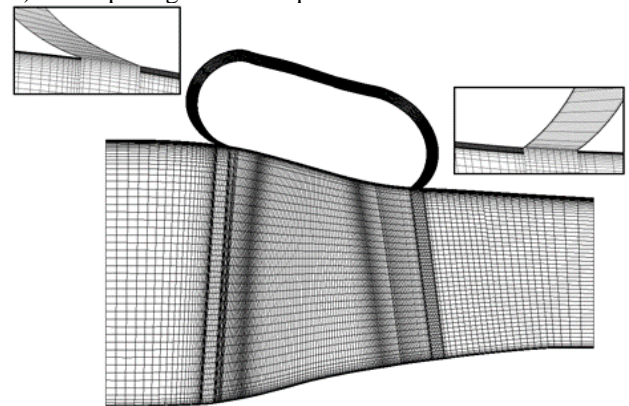
Figure 2 illustrates the mesh used for the rotor and the recirculation passageway. The rotor grid consists of three main blocks: inlet, outlet and the region around the blade. The inlet and outlet, as well as the recirculation passageway, have been simulated in the stationary frame. O-type grid has been used around the blade (163 x 19 nodes) and H-type one for the outer parts (201 x 59 x 89 nodes in the streamwise, circumferential and spanwise directions, respectively). The grid includes 33 nodes in the radial direction between the tip of the blade and the casing wall, in order to accurately describe the complicated endwall flow field. The recirculation passageway includes 241 and 38 nodes in the streamwise and radial directions, respectively. Similar to the rotor blades, both O and H-type grids were used for the anti-swirl vanes (with 134 nodes in the circumferential direction). Near the wall surfaces, y^+ has been kept less than or equal to one, by grid clustering. SST $k-\omega$ was chosen to be the turbulence model because this model has a good accuracy in high pressure-gradient flows and separations. To solve the URANS equations, the time step was set to be $3.232e-6$ sec, corresponding to 1080 time steps per rotor revolution (three time steps per each degree of rotation). Furthermore, 12 internal iterations were performed at each time step. The solid boundaries are assumed to be adiabatic. Total pressure, total temperature and flow angle are specified at the inlet (in accordance with the experimental data in Dunham (1998)). At the outlet, average static pressure integrated over the boundary is specified. Finally, periodic flow conditions were applied to the periodic boundaries both in the rotor and recirculation passageway.

3. RESULTS AND DISCUSSION

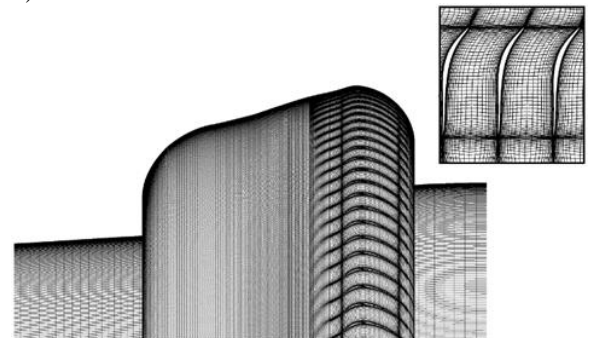
URANS equations have been solved for the smooth casing from the choking to stall conditions. To throttle from choking condition toward stall, the outlet static pressure was gradually increased. Time histories of the



a) Blade passage at 95 % span



b) Meridional view



c) Recirculation passageway and anti-swirl vanes

Fig. 2 Computational grid

rotor mass flow rate at the inlet and outlet were monitored during each calculation in order to ensure the convergence of the solution to a fully-developed stable operating condition. The near-stall point was determined to be the last stable operating point for which fully-developed condition could be achieved. The computational performance curves of the rotor are obtained by mass averaging the total pressure and total temperature at the rotor inlet and outlet. A comparison between the rotor experimental performance curves and the numerical ones (time-averaged) is given in Fig. 3. Note that the annulus mass flow at near stall point is roughly 93 percent of that at the design point. The choking mass flow rates (20.93 Kg/s for the experiments and 20.83 for the numerical

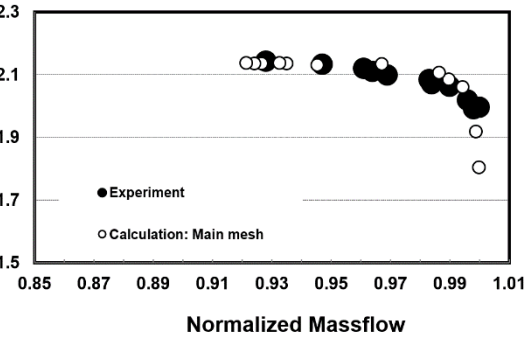
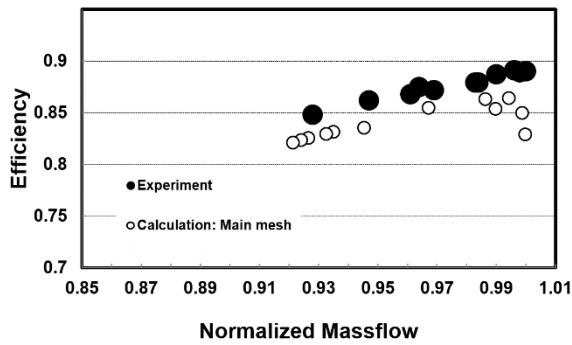


Fig. 3 Characteristics of rotor (smooth casing)

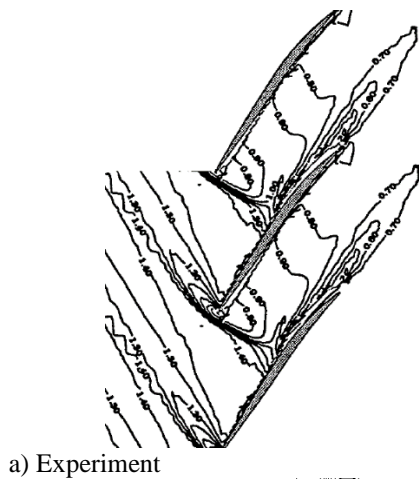
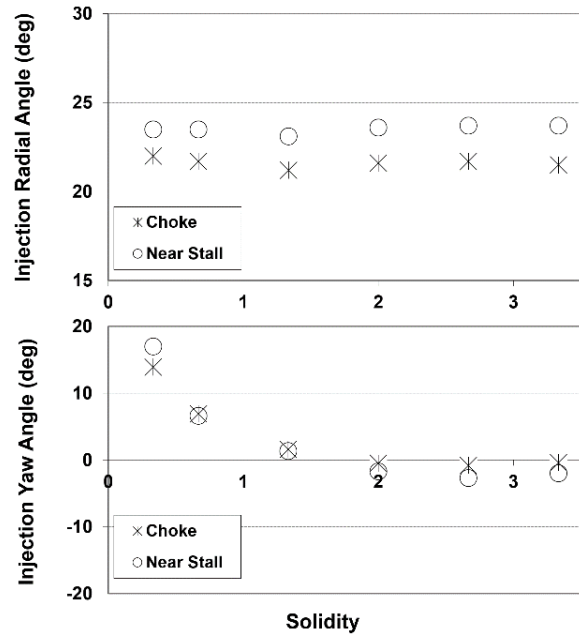
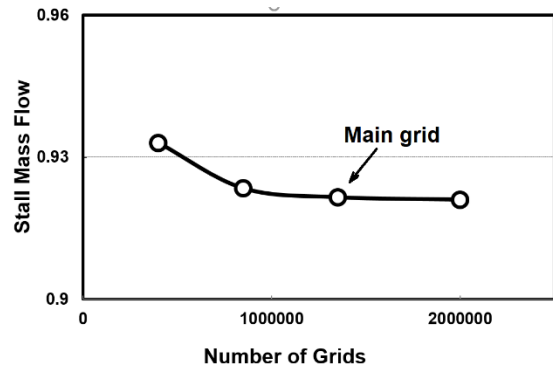


Fig. 4 Relative Mach number contours (70 % span at stall point)

calculations) have been used to normalize the mass flows in this figure. As Fig. 3 shows, the calculated rotor overall performance agrees quite well with the experimental data. In order to validate the accuracy of the calculations in predicting the compressor flow field, contours of relative



Mach number (time-averaged at 70 % span and near-stall condition) are illustrated in Fig. 4, which shows a quite accurate prediction. Mesh independency analysis is performed in this work, which is illustrated in Fig. 5 in terms of normalized stalling mass flow.

In order to find the optimum number of anti-swirl blades, steady simulations have been performed from choke to near-stall for six solidities of the guide vanes. Figure 6 shows the injection yaw and radial angles for different vane solidities, at choking and near-stall operating points. As shown in this figure, the injection radial angle is almost constant for all of the cases (roughly 21.5 deg and 23.5 deg at the choking and near-stall conditions, respectively). However, increasing the solidity of the guide vane from 0.333 to 2 considerably reduces the injection yaw angle (from roughly 17 deg to about zero). Figure 7 illustrates the total pressure loss of the recirculation passageway at the choking and near-stall conditions (from the bleed to injection port). The pressure losses in this figure are referenced to the ambient pressure (Eq. (1)).

$$\frac{(P_{0bleed} - P_{0inj})}{P_{amb}} \times 100 \quad (1)$$

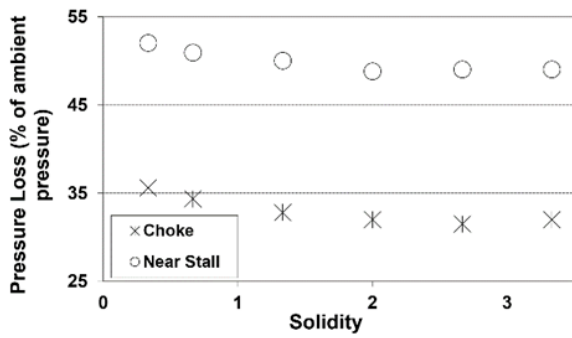


Fig. 7 Total pressure loss of the recirculation passageway

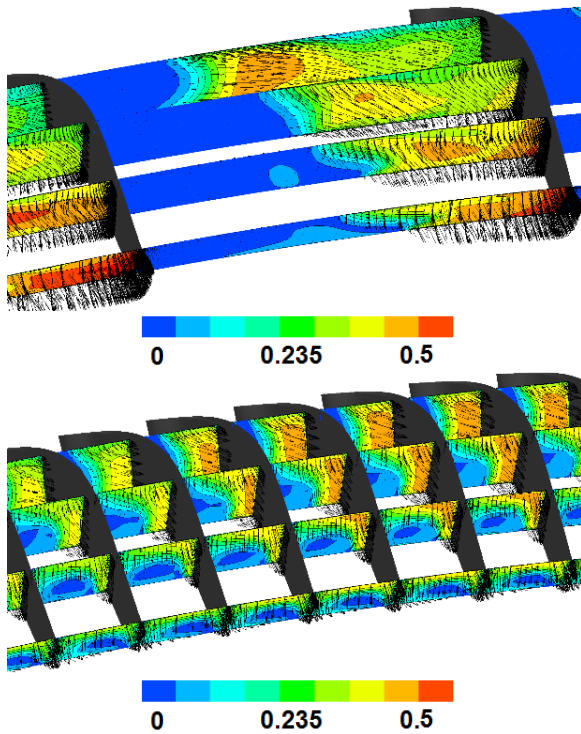


Fig. 8 Contours of Mach number between the vanes (top: 72 vanes, bottom: 360 vanes)

The minimum pressure loss is occurred for 216 guide vanes (solidity=2) and is equivalent to roughly 48.8 percent of ambient pressure at near-stall. Figure 8 shows contours of Mach number on four surfaces between the guide vanes and at near-stall. Two solidities are shown, 0.667 and 3.333. Large zones of separation can be observed on the suction surfaces of the blades for the two configurations shown, especially near the passage hub. However, the flow is more uniform for the greater solidity. The number of the anti-swirl vanes for unsteady computations has been chosen to be equivalent to 216 (solidity equivalent to 2), which was effective in removing the injection yaw angle and had minimum total pressure loss.

Unsteady calculations were performed for the treated casing with 216 guide vanes. The characteristic curves of the compressor adiabatic efficiency and total pressure ratio are given in Fig. 9. As this figure shows, considerable stability improvement (about 36 percent) has been achieved by the current recirculation casing treatment design. However, as Fig. 9 illustrates, this is attained at the

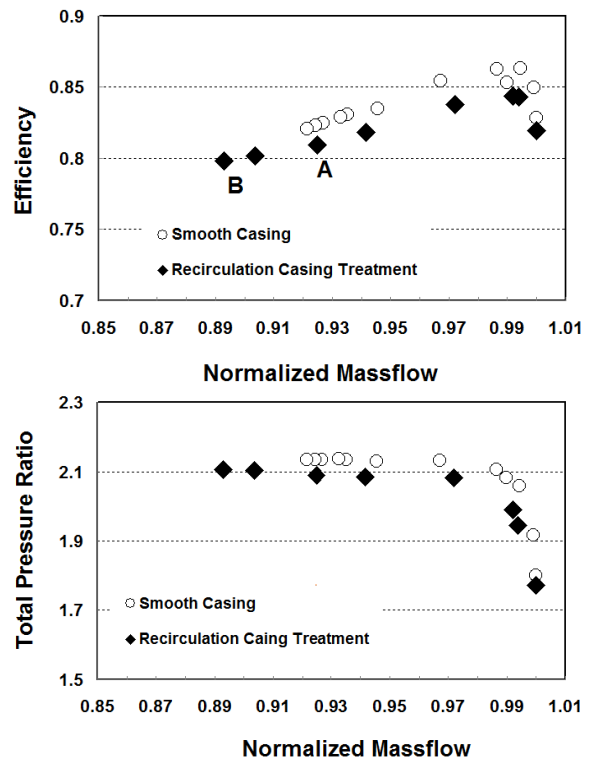


Fig. 9 Rotor characteristics (recirculation casing)

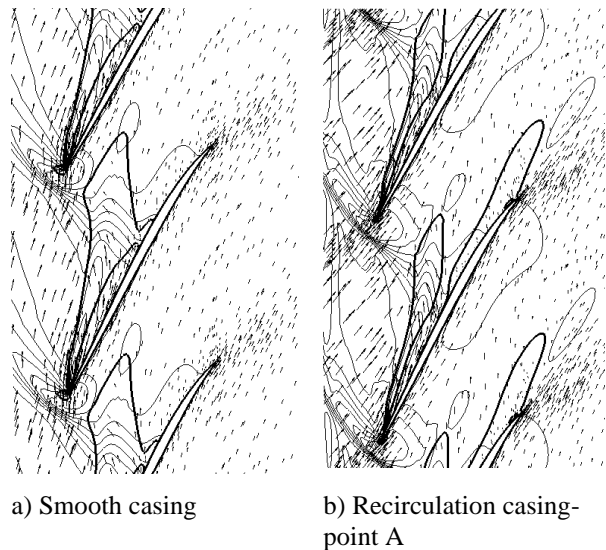
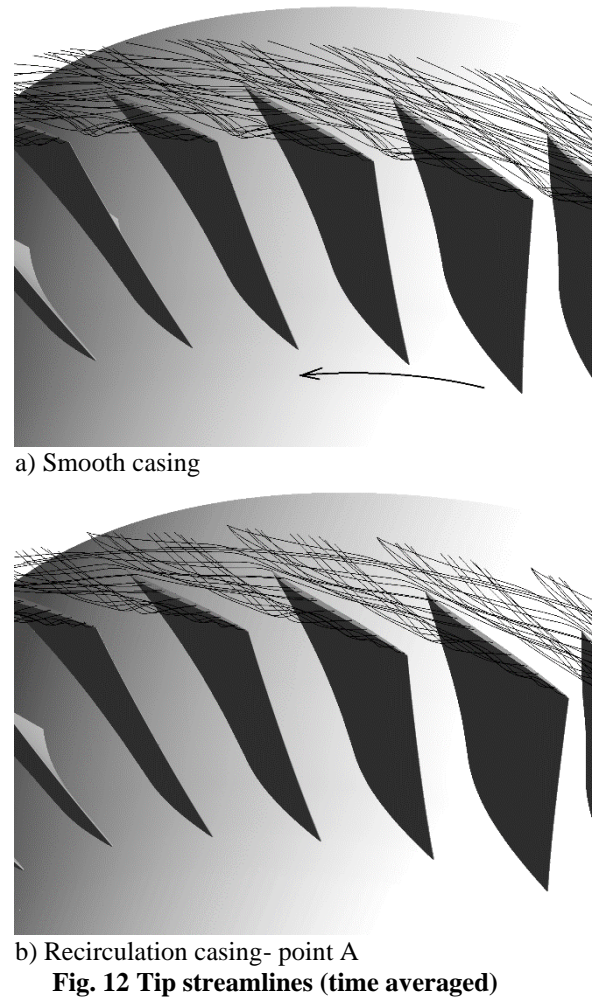
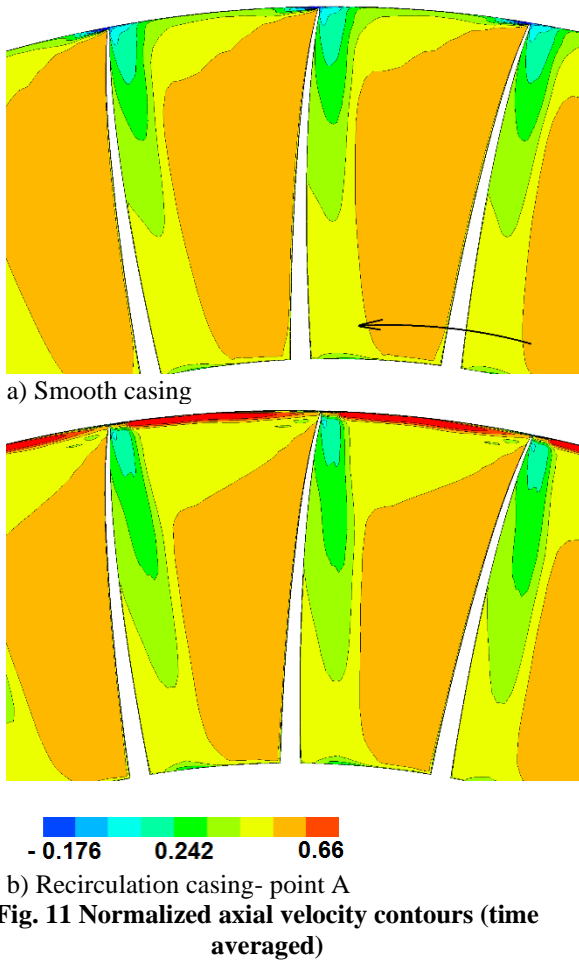


Fig. 10 Static pressure contours at blade tip (time averaged)

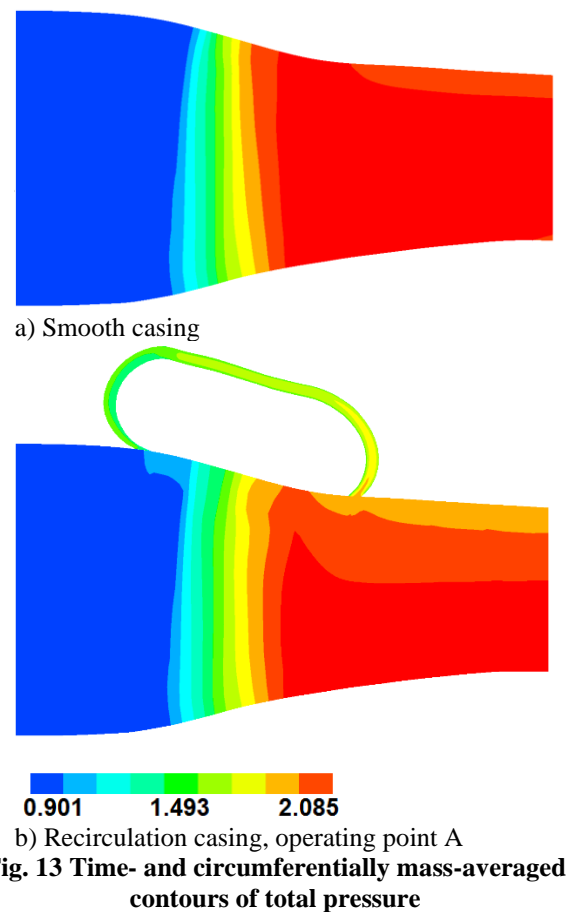
expense of some penalty in the compressor performance (both efficiency and total pressure ratio). Point A in this figure corresponds to the stall point of the smooth casing, and point B to the stall condition of the treated casing.

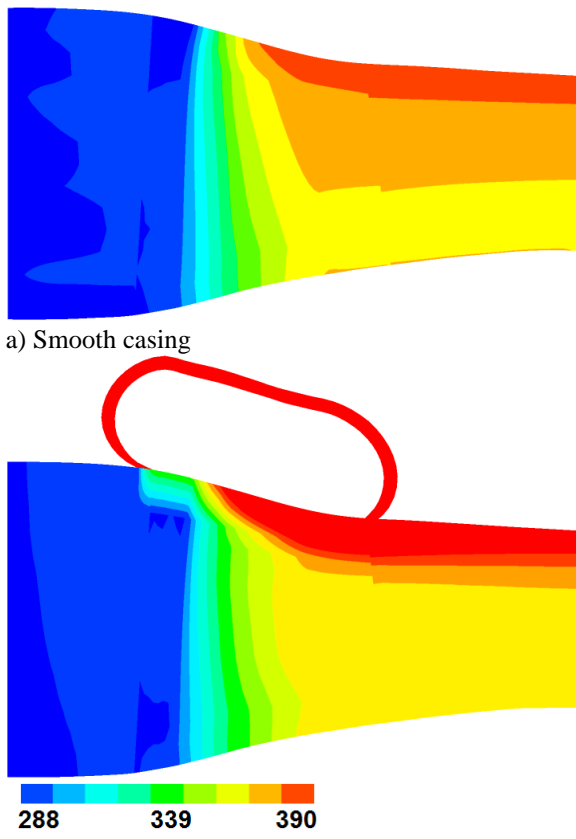
Figure 10 illustrated time-averaged static pressure contours at the blade tip (the smooth casing at the stall point and the treated rotor at points A). This figure also includes relative velocity vectors. Furthermore, zones of reverse flow are specified by using thick lines. Comparing the relative velocity vectors reveals that recirculation has considerably reduced the relative flow angles over the leading-edge of the blade. It is further observed in this figure that recirculation has pushed the reverse flow zones toward the blade trailing-edge. It was found by [Vo et al. \(2008\)](#).



that prior to spike initiated rotating stall, the interface between the leakage and main flows becomes parallel to the leading-edge plane. By injecting high velocity fluid upstream of the blades, this interface is pushed downstream and toward the blade suction surface, which postpones the occurrence of stall inception (see Fig. 10(b)). Figure 11 shows time-averaged axial velocity contours (normalized by the blade tip speed), just at the tip leading edge of the blade. The axial velocity contours near the blade tip clearly show the impact of recirculation in energizing endwall flow and removing the low momentum fluid, especially from the blade pressure surface endwall corner. Tip streamlines (time averaged) are plotted in Fig. 12 for the smooth and treated casings. This figure shows that recirculation has pushed the tip leakage vortex toward the blade suction surface, which is the key to stability enhancement, as mentioned above.

A comparison of the time-averaged contours of total pressure, between the smooth and recirculation casing, is given in Fig. 13. The total pressures in this figure are circumferentially mass-averaged. Furthermore, note that the total pressures are normalized by using the ambient pressure. The recirculation casing is shown at the near stall point of the smooth casing (operating point A). Similar contour plots of total temperature are shown in Fig. 14. The total temperatures in this figure are normalized by using the reference temperature, which is equivalent to 288 K. As seen in Fig. 13, recirculation of high pressure air has slightly increased the total pressure in front of the





a) Smooth casing
b) Recirculation casing, operating point A
Fig. 14 Time- and circumferentially mass-averaged contours of total temperature

injection port. However, it has reduced the exit total pressures, which is in accordance with the loss in the total pressure ratio observed in Fig. 9. As Fig. 14 shows, total temperature is increased at the compressor outlet in the treated compressor, as compared to the smooth casing. This increase in exit total temperature, together with the loss in the exit total pressure, explains why the adiabatic efficiency has dropped due to recirculation.

Figure 15 illustrates meridional velocity vectors and static and total pressure contours for the recirculation passageway at operating point B. Similar to Figs. 13 and 14, the properties in Fig. 15 are time- and circumferentially mass-averaged. As seen, the static pressure first increases gradually, due to the increase in the area of the passageway, and then remains almost constant up to the anti-swirl vanes. The static pressure is slightly increased by the vanes, but finally drops by decreasing the area at the injection port. On the other hand, the total pressure drops throughout the passageway, but mostly at the entrance to the channel and the anti-swirl vanes. This loss is partly originated from flow separation from the passageway surfaces (owing to the axial and radial velocity of the bled air), but also from flow separation from the suction surfaces of the vanes (due to the circumferential velocity of the circulated fluid). Note that the total pressure loss of the recirculation passageway was calculated by time- and mass-averaging the total pressures at the injection and bleed ports (Eq. (2)): roughly 20.5, 23 and 26.5 percent at the choking point and operating points A and B, respectively. As the velocity vectors in Fig. 15 suggest, air is injected with a radial angle relative to the

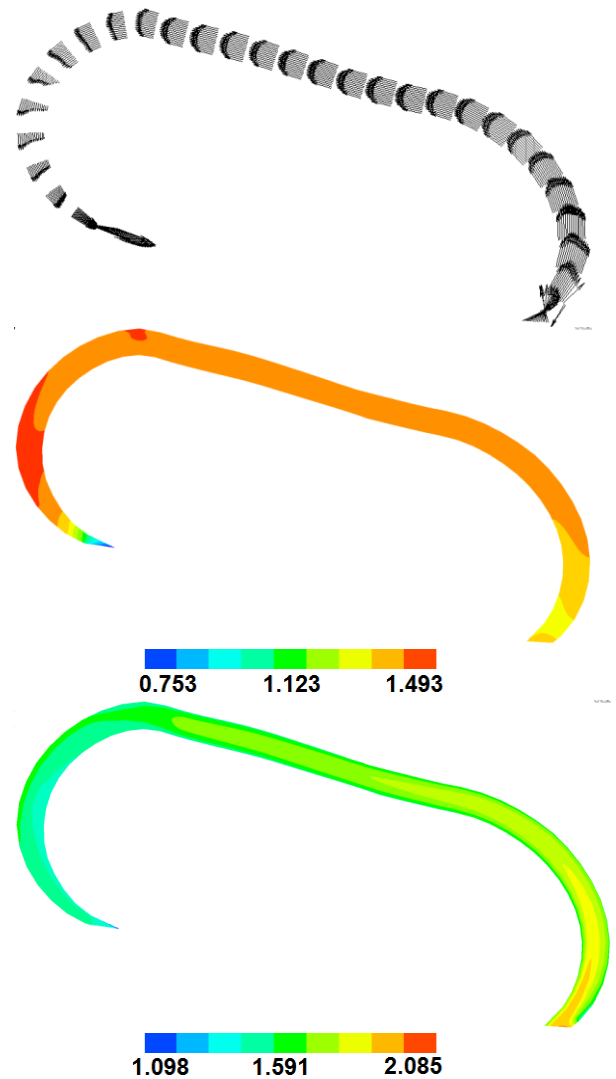


Fig. 15 Time- and circumferentially mass-averaged velocity vectors and static and total pressure contours in the recirculation passageway (operating point B)

axial direction, which was calculated (by time- and mass-averaging the velocities) and found to vary from roughly 21 deg at the choking point to 23.5 deg at the near-stall condition.

$$\frac{(P_{0bleed} - P_{0inj})}{P_{0bleed}} \times 100 \quad (2)$$

Figure 16 shows the time-averaged normalized total pressure and Mach number contours at point B and on a surface located at 50 percent height of the recirculation passage. The time-averaged velocity vectors are further added to these contour plots. Comparing the velocity vectors along the passage shows that the anti-swirl vanes used in the current study have effectively turned the bled air (with a very high circumferential velocity component) to the axial direction. The total pressure loss occurs throughout the passage, especially due to the flow separation from the suction surface of the vanes. Nonetheless, as observed in Fig. 16, the (time-averaged) Mach number at the injector exit is near one. This high-speed jet effectively reduced the endwall blockage and caused considerable range extension, as discussed earlier.

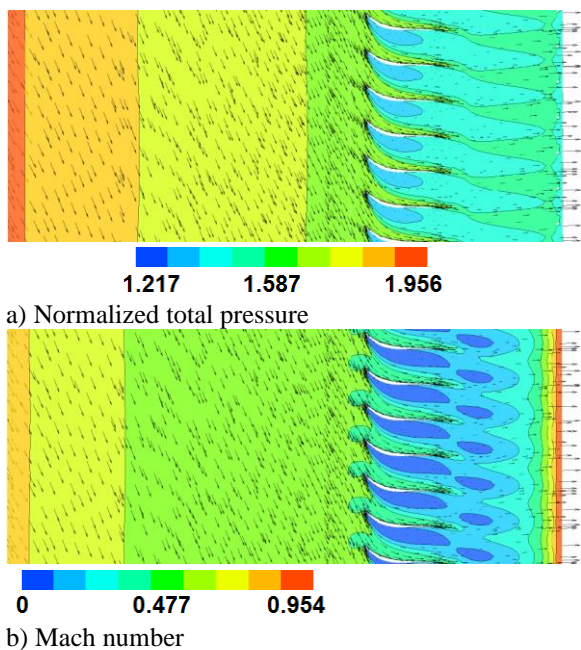


Fig. 16 Mach number contours and total pressure at 50 percent height of the recirculation passageway (time averaged at operating point B)

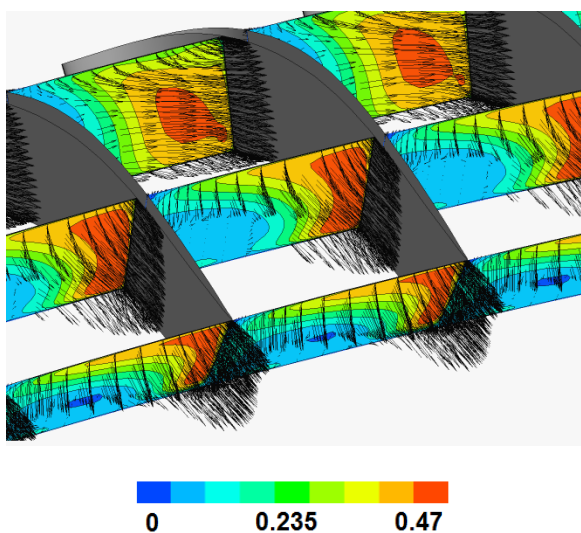


Fig. 17 Mach number contours between the vanes (time averaged at operating point B)

The time-averaged Mach number contours are shown on three surfaces between the vanes in Fig. 17 and at the same condition applied to Fig. 16. Furthermore, velocity vectors (time averaged) are shown in this figure to clarify the flow field and specify the reverse flow regions. As seen, flow separation (on the suction surface of the vanes) has created large reverse flow regions, especially near inner surface of the recirculation passageway. This is in agreement with the results presented in Fig. 15, because as shown in this figure, the averaged total pressures and velocities near the outer surface of the recirculation passageway are greater, as compared to the inner one.

Time histories of the injected mass flow (percent of the annulus mass flow rate) at operating points A and B are illustrated in Fig. 18. The average amount of recirculation is roughly 2.84 percent of the annulus flow at operating point A and 2.92 percent at point B. This figure shows some fluctuations in the injected mass flow,

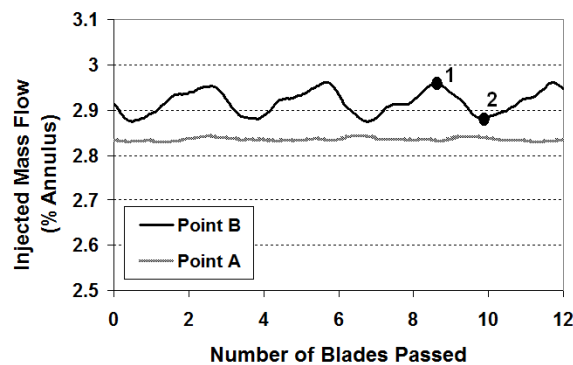
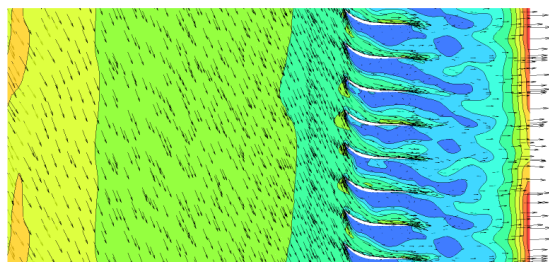


Fig. 18 Time histories of the injected mass flow rate

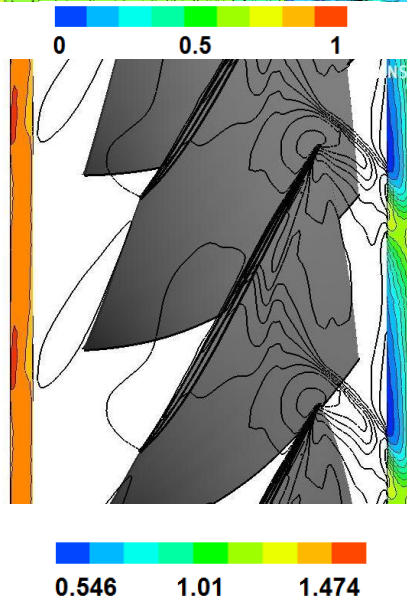
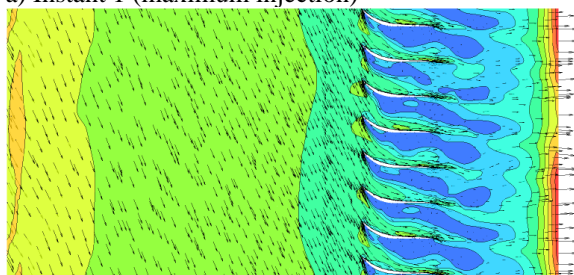
which is greater at operating point B (roughly 1.4 percent, as compared to the average injected mass flow rate). The reason for this unsteadiness is the interaction between the main passage shock and the injection port. In order to clarify this effect, instantaneous contour plots of Mach number are shown in Fig. 19 on the same surface which was used in Fig. 16 and at operating point B. To instants are shown in this figure: instants 1 and 2, which have been specified in Fig. 19 and correspond to the maximum and minimum injected mass flow rates, respectively. At each instant, static pressure contours are shown at the blade tip (also on injection/bleed ports). As shown in these figures, the passage shock-injection port interaction causes non-uniformity in the static pressure at the injection face, which in turn changes the Mach number at the injector exit. As the blade rotates, the injected mass flow rate fluctuates, which is due to the unsteady sources such as shock and leakage flow oscillations.

4. CONCLUSION

The effects of endwall air recirculation on the stability and performance of NASA Rotor 37 were studied in this investigation. An annular recirculation passageway was designed and located on the casing over the blades. Because the test case was an isolated compressor rotor, without any stator or outlet guide vanes, some anti-swirl vanes were placed within the passageway. Although these vanes caused some total pressure loss, they increased the injector effectiveness by removing the circumferential velocity component of the injected fluid. The effect of the solidity of the anti-swirl vanes has been studied in this work, to select the optimum solidity in terms of minimum pressure loss and maximum effectiveness in removing the swirl component. Results showed that the passageway used in this work can effectively provide a high-velocity jet of fluid in the axial direction. The total pressure loss of the recirculation passageway varied from about 20.5 percent at the choking condition to roughly 26.5 percent at the near-stall point. This loss was partly originated from flow separation from the recirculation passageway surfaces at its entrance (due to the axial and radial velocity components of the bled air), but also from flow separation on the suction surfaces of the anti-swirl vanes. It was also found that the interaction between the passage shock and the injection surface caused non-uniform static pressure distribution, which in turn resulted in non-uniform velocity distribution at the injector exit. Consequently, the circulated mass flow rate fluctuated by the blade rotation,



a) Instant 1 (maximum injection)



b) Instant 2 (minimum injection)

Fig. 19 Instantaneous Mach number contours: 50 % height of recirculation passageway, operating point B

which is due to unsteady sources such as shock wave and leakage flow oscillations. Results reveal that recirculation

reduce the incidence angle over the blade and push the passage shock and leakage vortex backward, which lead to stability improvement.

ACKNOWLEDGEMENTS

This work was partially supported by Iran National Science Foundation (INSF).

CONFLICT OF INTEREST

The authors have no conflict of interest to disclose.

AUTHORS CONTRIBUTION

M. J. Shahriyari: simulations, writing. **H. Khaleghi:** supervision, design, contributed to simulation and writing.

REFERENCES

- Akhlaghi, M., Elder, R. L., & Ramsden, K. W. (2003, January). *Effects of a vane-recessed tubular-passage passive stall control technique on a multistage, axial-flow compressor: results of tests on the first stage with the rear stages removed*. Turbo Expo: Power for Land, Sea, and Air. <https://doi.org/10.1115/GT2003-38301>
- Azimian, A. R., Elder, R. L., & McKenzie, A. B. (1990). Application of recess vaned casing treatment to axial flow fans, *Journal of Turbomachinery*, 112(1), 145-150. <https://doi.org/10.1115/1.2927411>
- Dinh, C. T., Ma, S. B., & Kim, K. Y. (2017, June). *Effects of a circumferential feed-back channel on aerodynamic performance of a single-stage transonic axial compressor*. Turbo Expo: Power for Land, Sea, and Air. American Society of Mechanical Engineers. <https://doi.org/10.1115/GT2017-63536>
- Dunham, J. (1998). *CFD validation for propulsion system components (la validation CFD des organes des propulseurs)*. Advisory Group For Aerospace Research And Development Neuilly-Sur-Seine (France).
- Freeman, C., Wilson, A. G., Day, I. J., & Swinbanks, M. A. (1998). Experiments in active control of stall on an aeroengine gas turbine. *Journal of Turbomachinery*, 120(4), 637-647. <https://doi.org/10.1115/1.2841773>
- Hathaway, M. D. (2002). *Self-recirculating casing treatment concept for enhanced compressor performance*. Conference Sponsors: International Gas Turbine Institute. <https://doi.org/10.1115/GT2002-30368>
- Hwang, Y., & Kang, S. H. (2013). Numerical study on near-stall flow unsteadiness in an axial compressor with casing treatment. *Journal of Mechanical Science and Technology*, 27(8), 2375-2381. <https://doi.org/10.1007/s12206-013-0622-9>
- Jahani, Z., Khaleghi, H., & Tabejamaat, S. (2022). Tip injection effects on a transonic centrifugal impeller

- with various tip clearances in the presence of inlet distortion. *Journal of the Brazilian Society of Mechanical Sciences and Engineering*, 44(9), 1-14. <https://doi.org/10.1007/s40430-022-03714-5>
- Khaleghi, H. (2014). Effect of discrete endwall recirculation on the stability of a high-speed compressor rotor. *Aerospace Science and Technology*, 37, 130-137. <https://doi.org/10.1016/j.ast.2014.05.009>
- Khaleghi, H. (2017). Parametric study of injector radial penetration on stalling characteristics of a transonic fan. *Aerospace Science and Technology*, 66, 112-118. <https://doi.org/10.1016/j.ast.2017.02.020>
- Khaleghi, H. (2020). A new approach of endwall recirculation in axial compressors. *Aerospace Science and Technology*, 98, 105704. <https://doi.org/10.1016/j.ast.2020.105704>
- Khaleghi, H., Heinrich, M., & Shahriyari, M. J. (2021). Circumferential casing treatment in a transonic fan. *Amirkabir Journal of Mechanical Engineering*, 53(7), 5-5. <https://doi.org/10.22060/mej.2021.18660.6879>
- Khaleghi, H., Teixeira, J. A., Tousi, A. M., & Boroomand, M. (2008). Parametric study of injection angle effects on stability enhancement of transonic axial compressors. *Journal of propulsion and power*, 24(5), 1100-1107. <https://doi.org/10.2514/1.34817>
- Khaleghi, H., Tousi, A. M., Boroomand, M., & Teixeira, J. A. (2007). Recirculation casing treatment by using a vaned passage for a transonic axial-flow compressor. *Proceedings of the Institution of Mechanical Engineers, Part A: Journal of Power and Energy*, 221(8), 1153-1162. <https://doi.org/10.1243/09576509JPE444>
- Lim, H. S., Bae, H. J., Lim, Y. C., Song, S. J., Kang, S. H., & Yang, S. S. (2011). Injection profile effects on low speed axial compressor stability enhancement. *Journal of Mechanical Science and Technology*, 25(6), 1501-1507. <https://doi.org/10.1007/s12206-011-0332-0>
- Puterbaugh, S. L., & Brendel, M. (1997). Tip clearance flow-shock interaction in a transonic compressor rotor. *Journal of Propulsion and Power*, 13(1), 24-30. <https://doi.org/10.2514/2.5146>
- Reid, L., & Moore, R. D. (1978). *Design and overall performance of four highly loaded, high speed inlet stages for an advanced high-pressure-ratio core compressor* (No. NASA-TP-1337).
- Reid, L., & Moore, R. D. (1979, January). *Experimental study of low aspect ratio compressor blading*. Ann. Intern. Gas Turbine Conf. (No. NASA-TM-79280).
- Strazisar, A. J., Bright, M. M., Thorp, S., Culley, D. E., & Suder, K. L. (2004, January). *Compressor stall control through endwall recirculation*. Turbo Expo: Power for Land, Sea, and Air. <https://doi.org/10.1115/GT2004-54295>
- Suder, K. L., Hathaway, M. D., Thorp, S. A., Strazisar, A. J., & Bright, M. B. (2001). Compressor stability enhancement using discrete tip injection. *Journal of Turbomachinery*, 123(1), 14-23. <https://doi.org/10.1115/1.1330272>
- Talebnezhad, M. (2017). *Numerical study of endwall recirculation on the performance of a high speed compressor* [MSc Thesis, Amirkabir University of Technology].
- Tang, Q., Wu, H., Li, J., Lou, H., & Yang, C. (2022). Performance optimization of centrifugal compressors based on throughflow model. *Arabian Journal for Science and Engineering*, 47(12), 16439-16450. <https://doi.org/10.1007/s13369-022-06736-2>
- Vo, H. D., Tan, C. S., & Greitzer, E. M. (2008). Criteria for spike initiated rotating stall. *Journal of Turbomachinery*, 130(1), 011023. <https://doi.org/10.1115/1.2750674>
- Vuong, T. D., & Kim, K. Y. (2021). Design optimization of a dual-bleeding recirculation channel to enhance operating stability of a transonic axial compressor. *Energies*, 15(1), 159. <https://doi.org/10.3390/en15010159>
- Wang, W., Chu, W., & Zhang, H. (2018). Mechanism study of performance enhancement in a subsonic axial flow compressor with recirculating casing treatment. *Proceedings of the Institution of Mechanical Engineers, Part G: Journal of Aerospace Engineering*, 232(4), 680-693. <https://doi.org/10.1177/0954410016687140>
- Weigl, H. J., Paduano, J. D., Frechette, L. G., Epstein, A. H., Greitzer, E. M., Bright, M. M., & Strazisar, A. J. (1997). *Active stabilization of rotating stall and surge in a transonic single stage axial compressor*. American Society of Mechanical Engineers. <https://doi.org/10.1115/97-GT-411>
- Xiang, H., Chen, J., Cheng, J., Niu, H., Liu, Y., & Song, X. (2021). Aerodynamic improved design and optimization for the rear stage of a High-load axial compressor. *Journal of the Brazilian Society of Mechanical Sciences and Engineering*, 43(3), 1-20. <https://doi.org/10.1007/s40430-021-02848-2>
- Yan, S., & Chu, W. (2020). Influence of self-circulating casing treatment with double-bleed ports structure on compressor performance. *Proceedings of the Institution of Mechanical Engineers, Part G: Journal of Aerospace Engineering*, 234(11), 1743-1756. <https://doi.org/10.1177/0954410020918405>
- Yang, C., Wu, H., & Liang, Y. (2019). A novel three-dimensional inverse method for axial compressor blade surface design. *Arabian Journal for Science and Engineering*, 44, 10169-10179. <https://doi.org/10.1007/s13369-019-04083-3>
- Zhou, J., Hou, A., & Zhou, S. (2010). Effects of injection frequency on the rotor stall margin. *Science in China Series E: Technological Sciences*, 53(1), 213-219. <https://doi.org/10.1007/s11431-010-0033-4>